Transactions of JASCOME Vol. 20 (Dec. 2020), Paper No. 10-201219 JASCOME

Level-set based topology optimization for heat conduction problem using lattice Boltzmann method

Truong NGUYEN[1)], Hiroshi ISAKARI[2)], Toru TAKAHASHI[3)], Masato YOSHINO[4)], Toshiro MATSUMOTO[5)]

1) Nagoya University (Furo-cho, Chikusa-ku, Nagoya, Aichi, 464-8601, E-mail: truongnguyen@nuem.nagoya-u.ac.jp)
2) Nagoya University (Furo-cho, Chikusa-ku, Nagoya, Aichi, 464-8601, E-mail: isakari@nuem.nagoya-u.ac.jp)
3) Nagoya University (Furo-cho, Chikusa-ku, Nagoya, Aichi, 464-8601, E-mail: ttaka@nuem.nagoya-u.ac.jp)
4) Shinshu University (4-17-1 Wakasato , Nagano, Nagano 380-8553, E-mail: masato@shinshu-u.ac.jp)
5) Nagoya University (Furo-cho, Chikusa-ku, Nagoya, Aichi, 464-8601, E-mail: t.matsumoto@nuem.nagoya-u.ac.jp)

This study aims to contribute to the expansion of the topology optimization for the heat conduction problem. The optimization is based on the level-set function to explicitly express the material distribution. Besides, the lattice Boltzmann method of low computation cost is used as a heat conduction solver to exploit its simplicity in the implementation as a simulation method with reasonable accuracy. The applicability of the collaboration between the lattice Boltzmann method and topological derivative in the topology optimization for the heat conduction problem in this study was verified through several numerical examples. Its computational efficiency is, moreover, compared with the existing methods in literature.

Key Words: Topology optimization, Level-set method, Lattice Boltzmann method, Heat conduction, Adjoint problem, Topological derivative

1. Introduction

Controlling the temperature of devices in operation plays an important role in the improvement of its performance and the life-time of equipments. There are various ways of regulating the temperature of devices. Among the solutions, the heat conduction tools (e.g. heat sink, heat pipes, and so on) with high conductivity are widely accepted. Therefore, the development of the heat conductive structure with a high ability of thermal diffusion and the low material fraction is attractive. Recently, topology optimization for the thermal conductor for dissipating heat is becoming an up-and-coming way for producing conceptual design in various engineering applications.

In general, the topology optimization of heat conduction has been extensively developed in a number of publications, in which various methods were used in the optimization. Regarding the established topology optimization methods for heat conduction, it can be classified into several different approaches, including the density based approach (1) (2) (3) (4) (5) (6) (7) (8) (9) (10), the evolutionary structural optimization (ESO) (11) (12), and the level-set based method (13) (14) (15) (16) (17) (18). The readers may also refer to a review paper (19) for more information in historical literature of topology optimization for heat conduction problem.

In a different aspect, the aforementioned studies mainly used the conventional methods in the optimization for heat conduction problems, such as finite difference method (FDM), finite element method (FEM), finite volume method (FVM), and boundary element method (BEM). It is, however, quite challenging in dealing with a large-scale optimization problem, especially, for the problem consisting of design dependent boundaries on which some explicit boundary conditions are specified. Moreover, the iterative update in shapes during the optimization process requires a lot of computational cost for re-meshing and re-calculation process. Therefore, the use of those conventional methods in such a problem needs high computation resources.

Alternatively, in the last few decades, the lattice Boltzmann method (LBM) has been recognized as a substitute for simulating many problems in physics, such as incompress-

Received Oct. 21, 2020, accepted Nov. 14, 2020

ible flows [20] [21] [22], compressible flows [23] [24], complex systems [25], and simulation of other partial differential equations, such as Laplace's equation [26] [27], Poisson's equation [28] [29], the Poisson-Boltzmann equation [30], and reaction-diffusion equation [31]. Moreover, the LBM has successfully been used in topology optimizations of various application fields, e.g. steady Navier-Stokes problem [32] [33] [34], unsteady Navier-Stokes problem [35] [36] [37] [38], and heat transfer problem [39] [40] [41].

As shown in the recent review paper by Dbouk et al. (2017) and the current reviews on the literature of engineering design for heat conduction systems, the use of LBM in topology optimization for heat conduction problems has not directly been performed. Hence, the potential paradigm of collaborating the LBM in the topology optimization for the heat conduction problem is attracting wide attention. Moreover, in the optimization of the heat conduction using LBM, one of the elements to consider over the conventional methods is that the simplicity of its algorithm, particularly, the numerical simplicity of handling the complex boundaries. Also, the noticeable advantage of using LBM is its parallel computation of complex and large-scale problems. However, instead of exploiting the advantages of LBM, the aforementioned authors preferably used conventional simulation methods for optimization.

Furthermore, it is shown in the recent study by Jing et al. (2015) that the optimization was solved by using the reaction-diffusion level-set function [42] in which the topological sensitivity information of the objective function represents the reaction term in the implicit time evolution level-set function. In the study, the topological derivative of the objective function is determined with respect to the topological perturbation caused by an infinitesimal circular region removed from the material domain. The calculation of the topological derivative was done by the computation of the primal variables that correspond to Laplace's equation and the adjoint problem corresponding to Poisson's equation using BEM. Therefore, in this study, we aim at testing the applicability and the computational efficiency of the topology optimization for heat conduction problems wherein both the primal and adjoint problems are solved by using the standard regularized Bhatnagar-Gross-Krook LBM vice versa. The cooperation between LBM and the topological derivative concept in the optimization for the heat conduction problem is also tested through various numerical examples in this study.

Besides, the LBM has already been used in a few studies for topology optimization for the heat transfer problem. Even though the topology optimization for the heat transfer problem as compared to the heat conduction problem is fairly different, it can be modified in straight forward manner to solve the heat conduction problem. To be more specific, the heat transfer problem becomes a pure heat diffusion process if there is no impact of the fluid flow on the thermal field. The fluid velocity is, therefore, simplified to zero in this case. However, concerning the topology optimization for heat conduction problem using LBM in literature, the aforementioned authors used the continuous sensitivity analysis instead of the topological derivative to compute the gradient of the objective function wherein the computation is based on the discrete adjoint lattice Boltzmann method (Rokicki et al., 2016) or the continuous adjoint lattice Boltzmann method (Yaji et al., 2016; Dugast et al., 2018) in the optimization. Particularly, in the aforementioned studies, the objective function is defined in terms of the distribution function. The gradient of the objective function is, therefore, computed with respect to the variation of objective function caused by a small perturbation of the distribution function at a particular point. This conception is somehow an approximation of the topological derivative wherein the variation of the level-set distribution at a point results in the topological variation. Thus, in this study, we present a more rigorous level-set based topology optimization for the heat conduction problem using LBM and cooperate with the topological derivative to validate them.

This paper is organized as follows. Section 2 shows the formulations of the topology optimization based on the level-set method wherein the primal problem and the adjoint problem, then the topological derivative is presented. The brief introduction of the chosen LBMs for solving the primal and adjoint problems are also contained in this section. In section 3, the validation of the constructed LBM and the validity of the use of the LBM in the topology optimization for the heat conduction problem are performed with different numerical examples. In the last section, the summaries of achievement in the study are conducted. We also point out some problems that need to be considered in future studies.

2. Formulation

2.1. Level-set based topology optimization problem

The level-set method is a numerical tool for expressing the distribution of material domain Ω, the non-material domain $D\backslash\Omega$, and the interface between them $\partial\Omega$ in the fixed domain D. The scalar level-set function $\phi(\mathbf{x})$ here, is defined as follows:

$$\begin{cases} 0 < \phi(\mathbf{x}) \leq 1 & \mathbf{x} \in \Omega\backslash\partial\Omega, \\ \phi(\mathbf{x}) = 0 & \mathbf{x} \in \partial\Omega, \\ -1 \leq \phi(\mathbf{x}) < 0 & \mathbf{x} \in D\backslash\Omega. \end{cases} \tag{1}$$

In this study, the characteristic function is associated with the level-set function as follows:

$$\chi_\phi(\mathbf{x}) = \begin{cases} 1 & \text{if} \quad \phi(\mathbf{x}) \geq 0, \\ 0 & \text{if} \quad \phi(\mathbf{x}) < 0. \end{cases} \tag{2}$$

Next, we consider the topology optimization for minimizing an objective function J. It is defined on the boundary and/or in the material domain as follows:

$$\min_{\phi} J(\chi_\phi) = \int_{\Omega} J_\Omega(u)\ d\Omega + \int_{\Gamma} J_\Gamma(u, q)\ d\Gamma,$$

subject to

$$\begin{aligned} &-k\nabla^2 u = 0 && \text{in } \Omega\backslash\partial\Omega, \\ &u = \bar{u} && \text{on } \Gamma_D, \\ &q = -k\frac{\partial u}{\partial n} = \bar{q} && \text{on } \Gamma_N, \\ &q = h(u - u_\infty) && \text{on } \Gamma_h, \end{aligned} \tag{3}$$

and

$$V = \int_{D} \chi_\phi d\Omega - V_{\max} \leq 0, \tag{4}$$

where $J_\Omega(u)$ and $J_\Gamma(u, q)$ denote the objective functions defined in the material domain and boundary, respectively. u denotes temperature, q denotes normal heat flux with thermal conductivity k, n denotes the outward normal vector with respect to Ω, h denotes the heat transfer coefficient on the Robin boundary Γ_h, u_∞ denotes ambient temperature, and $V_{\max}$ denotes the upper limit of the optimal material volume. The prescribed temperature imposed on the Dirichlet boundary Γ_D is denoted as $\bar{u}$ and the prescribed heat flux imposed on the Neumann boundary Γ_q is denoted as $\bar{q}$.

The problem of searching for a feasible shape that fulfills the equality and inequality constraints in the above equations (3) turns out to the problem of finding the optimal material distribution by solving the following reaction-diffusion level-set equation (Yamada et al., 2010). In the following time evolution equation, the gradient of the objective function J that represents in the reaction term gives a very important sense to predict an optimized shape, and the diffusion term plays a role of controlling the smoothness of the optimized shape. It is shown as follows:

$$\begin{aligned} &\frac{\partial \phi}{\partial t} = K\left(\mathcal{T} + \tau\nabla^2\phi\right) && \text{in } D, \\ &\phi|_{t=0} = \phi_0 && \text{in } D, \\ &\frac{\partial \phi}{\partial n} = 0 && \text{on } \partial D\backslash\Gamma_w, \\ &\phi = 1 && \text{on } \Gamma_w, \end{aligned} \tag{5}$$

where $K > 0$ is a proportional constant, τ denotes a regularization parameter, ϕ_0 denotes initial level-set function at fictitious time $t = 0$, Γ_w denotes the non-design boundary and $\mathcal{T}$ denotes the topological derivative that represents the sensitivity information of a given objective function. It is noted that the complete derivation of the topological derivative for the heat conduction was presented in the previous study by Jing et al. (2015). In that study, the authors used the adjoint method to express the topological derivative in which the heat transfer boundary condition is applied on the new boundary corresponding to a topological change.

The corresponding boundary value problem for the adjoint field μ is given as follows:

$$\begin{aligned} &-k\nabla^2\mu = \frac{\partial J_\Omega}{\partial u} && \text{in } \Omega, \\ &\mu = -\frac{\partial J_\Gamma}{\partial q} && \text{on } \Gamma_D, \\ &\eta = \frac{\partial J_\Gamma}{\partial u} && \text{on } \Gamma_N, \\ &\eta = h\left(\mu + \frac{\partial J_\Gamma}{\partial q} + \frac{1}{h}\frac{\partial J_\Gamma}{\partial u}\right) && \text{on } \Gamma_h, \end{aligned} \tag{6}$$

where

$$\eta = -k\frac{\partial \mu}{\partial n}. \tag{7}$$

It is noted that in the case of the objective function is defined only on the boundary, the gradient with respect to the temperature of the objective function defined in the material domain ($\frac{\partial J_\Omega}{\partial u}$) equals zero. Therefore, the adjoint problem is simplified to the Laplace's equation instead of the Poisson's equation as in Eq. (6).

As a result, the topological derivative can be computed as follows:

$$\mathcal{T} = \mu^0 h\left(u^0 - u_\infty\right) + \left(u^0 - \hat{u}\right)^2, \tag{8}$$

here u^0 and μ^0 are the temperature and temperature adjoint at the center of Ω_ϵ – an infinitesimal material domain, of the expanded u and μ, respectively, and $\hat{u}$ denotes the target temperature. The objective function $J_\Gamma = |u - \hat{u}|^2$ is implicitly used in the analysis. For more detail on the topological derivative procedure, the readers may refer to Jing et al. (2015).

2.2. Lattice Boltzmann method

2.2.1. Method of computation

In this study, the standard two-dimensional nine-velocity (D2V9) lattice Boltzmann method is used to obtain the primal solution u in the Laplace's equation (3) and the adjoint solution μ in the Poisson's equation (6). It is noted that the two-dimensional five-velocity (D2V5) lattice model is also a candidate to solve these Laplace's and Poisson's equations. However, for the wide-range applicabilities to the complex geometry design problems wherein the Robin boundary condition is employed, the D2V9 is selected in purpose in this study [(27)].

The characteristic particle velocity $\mathbf{c}_i$ and the weighting function w_i in the D2V9 lattice Boltzmann model read as follows:

$$\begin{aligned}&\left[\mathbf{c}_1, \mathbf{c}_2, \mathbf{c}_3, \mathbf{c}_4, \mathbf{c}_5, \mathbf{c}_6, \mathbf{c}_7, \mathbf{c}_8, \mathbf{c}_9\right] \\ &= \begin{bmatrix} 0 & 1 & 0 & -1 & 0 & 1 & -1 & -1 & 1 \\ 0 & 0 & 1 & 0 & -1 & 1 & 1 & -1 & -1 \end{bmatrix}.\end{aligned} \tag{9}$$

$$w_1 = 4/9, \ w_{2\text{-}5} = 1/9, \ w_{6\text{-}9} = 1/36. \tag{10}$$

The time evolution equation of the temperature distribution functions, $f_i(\mathbf{x}, t)$ that corresponds to the primal problem (3) and the adjoint temperature distribution functions $g_i(\mathbf{x}, t)$ that corresponds to the adjoint problem (6) read the following equations:

$$f_i(\mathbf{x} + \mathbf{c}_i \Delta x, t + \Delta t) - f_i(\mathbf{x}, t) = -\frac{1}{\tau_f}\left[f_i(\mathbf{x}, t) - f_i^{\mathrm{eq}}(\mathbf{x}, t)\right]. \tag{11}$$

$$\begin{aligned}g_i(\mathbf{x} + \mathbf{c}_i \Delta x, t + \Delta t) - g_i(\mathbf{x}, t) = &-\frac{1}{\tau_g}\left[g_i(\mathbf{x}, t) - g_i^{\mathrm{eq}}(\mathbf{x}, t)\right] \\ &+ \Omega_i'(\mathbf{x}, t).\end{aligned} \tag{12}$$

Here Δx and Δt denote the lattice spacing and the time step, respectively. τ_f and τ_g denote single relaxation times. $\Omega_i'(\mathbf{x}, t) = \Delta x w_i R D_{\sigma^*}$ denotes the force term, where D_{σ^*} is the thermal diffusivity and R is exactly the same as the right hand-side term in the Poisson's equation (6). $f_i^{\mathrm{eq}}(\mathbf{x}, t)$ and $g_i^{\mathrm{eq}}(\mathbf{x}, t)$ are the chosen equilibrium distribution functions designed as follows [(28) (43)]:

$$f_i^{\mathrm{eq}} = w_i u \quad \text{for} \quad i = 1, 2, 3, ...9. \tag{13}$$

$$g_i^{\mathrm{eq}} = w_i \mu \quad \text{for} \quad i = 1, 2, 3, ...9. \tag{14}$$

The macroscopic variables u and μ are computed as the thermal concentrations in terms of the distribution function $f_i(\mathbf{x}, t)$ and $g_i(\mathbf{x}, t)$, respectively, as follows:

$$u = \sum_{i=1}^{9} f_i = \sum_{i=1}^{9} f_i^{\mathrm{eq}} \tag{15}$$

$$\mu = \sum_{i=1}^{9} g_i = \sum_{i=1}^{9} g_i^{\mathrm{eq}} \tag{16}$$

In this study, the thermal diffusivities in the time evolution equations (11) and (12) are computed by the following formulas:

$$D_\sigma = \frac{1}{3}\left(\tau_f - \frac{1}{2}\right)\Delta x, \tag{17}$$

$$D_{\sigma^*} = \frac{1}{3}\left(\tau_g - \frac{1}{2}\right)\Delta x. \tag{18}$$

Moreover, as it is stated in the prevous studies (e.g Inamuro et al. [(44)], the thermal conductivities in the time evolution equations (11) and (12) are given as follows:

$$k = \frac{1}{3}\tau_f \Delta x, \tag{19}$$

$$k^* = \frac{1}{3}\tau_g \Delta x. \tag{20}$$

2.2.2. Boundary condition

In this section, the three typical types of heat conduction boundary conditions defined on the surfaces are presented. All the boundary conditions will be described in terms of the particle distribution function f_i for the primal problem. The similar procedures can be applied for those boundary conditions of the adjoint problem wherein the particle distribution function g_i must be treated in the same manner as f_i. In the lattice Boltzmann method, due to the characteristics of the propagation rules for those particles located on the boundary nodes, the temperature distribution functions at the boundary nodes must be specified and satisfied that $(\mathbf{c}_i \cdot \mathbf{n}) > 0$ are unknown. As shown in Fig. 1, we assume that the boundary node placed on the vertical line Γ_{wall} (at $x = 0$) and $\mathbf{n}$ is the unit normal vector [(43)]. The unknown temperature distribution functions f_i^{unknown} at the boundary node are given as follows:

$$f_i^{\mathrm{unknown}} = w_i \bar{u}' \quad \text{for} \quad (\mathbf{c}_i \cdot \mathbf{n}) > 0, \tag{21}$$

where $\bar{u}'$ is the thermal concentration of the unknown temperature distribution functions.

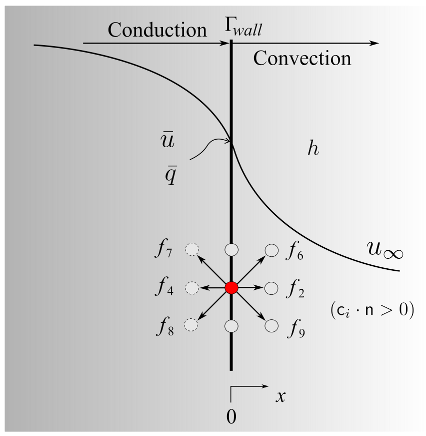

Fig. 1 Demonstration of the boundary conditions. The prescribed temperature $\bar{u}$ or the prescribed normal heat flux $\bar{q}$ will be specified at the boundary node in case of the Dirichlet or Neumann boundary conditions, respectively. The heat transfer coefficient h and the ambient temperature u_∞ are given in case of Robin boundary condition.

A. Dirichlet boundary condition: The Dirichlet boundary condition is imposed on the surface when the prescribed temperature $\bar{u}$ is specified at the boundary node. The unknown temperature distribution functions f_i^{unknown} can be derived by the equations as follows:

$$\begin{aligned}\bar{u} &= \sum\nolimits_{i(\mathbf{c}_i \cdot \mathbf{n} > 0)} f_i + \sum\nolimits_{i(\mathbf{c}_i \cdot \mathbf{n} \leq 0)} f_i \\ &= \left(\sum\nolimits_{i(\mathbf{c}_i \cdot \mathbf{n} > 0)} w_i\right)\bar{u}' + \sum\nolimits_{i(\mathbf{c}_i \cdot \mathbf{n} \leq 0)} f_i.\end{aligned} \tag{22}$$

$$\bar{u}' = \frac{\bar{u} - \sum_{i(\mathbf{c}_i\cdot\mathbf{n}\leq 0)} f_i}{\sum_{i(\mathbf{c}_i\cdot\mathbf{n}>0)} w_i}. \tag{23}$$

$$f_i^{\text{unknown}} = w_i \frac{\bar{u} - \sum_{i(\mathbf{c}_i\cdot\mathbf{n}\leq 0)} f_i}{\sum_{i(\mathbf{c}_i\cdot\mathbf{n}>0)} w_i}. \tag{24}$$

B. Neumann boundary condition: Similarly, the Neumann boundary condition is imposed on the surface when the normal heat flux $\bar{q}$ is prescribed at the boundary node. The normal heat flux can be obtained from the equilibrium distribution moments and described in Yoshino and Inamuro et al. (2003) such that $\bar{q} = \sum_{i=1}^{9} f_i \mathbf{c}_i \cdot \mathbf{n}$. The following equations are derived for the expression of the unknown temperature distribution functions:

$$\begin{aligned}\bar{q} &= \sum_{i(\mathbf{c}_i\cdot\mathbf{n}>0)} f_i \mathbf{c}_i\cdot\mathbf{n} + \sum_{i(\mathbf{c}_i\cdot\mathbf{n}\leq 0)} f_i \mathbf{c}_i\cdot\mathbf{n} \\ &= \left(\sum_{i(\mathbf{c}_i\cdot\mathbf{n}>0)} w_i \mathbf{c}_i\cdot\mathbf{n}\right)\bar{u}' + \sum_{i(\mathbf{c}_i\cdot\mathbf{n}\leq 0)} f_i \mathbf{c}_i\cdot\mathbf{n}.\end{aligned} \tag{25}$$

$$\bar{u}' = \frac{\bar{q} - \sum_{i(\mathbf{c}_i\cdot\mathbf{n}\leq 0)} f_i \mathbf{c}_i\cdot\mathbf{n}}{\sum_{i(\mathbf{c}_i\cdot\mathbf{n}>0)} w_i \mathbf{c}_i\cdot\mathbf{n}}. \tag{26}$$

$$f_i^{\text{unknown}} = w_i \frac{\bar{q} - \sum_{i(\mathbf{c}_i\cdot\mathbf{n}\leq 0)} f_i \mathbf{c}_i\cdot\mathbf{n}}{\sum_{i(\mathbf{c}_i\cdot\mathbf{n}>0)} w_i \mathbf{c}_i\cdot\mathbf{n}}. \tag{27}$$

C. Robin boundary condition: When the Robin boundary condition is imposed on the surface, the unknown temperature distributions at the boundary node will be expressed in terms of the known temperature distribution functions. This part is motivated by the study by Hiorth et al. (2009). The Robin boundary condition is formed as follows:

$$-k\mathbf{n}\cdot\nabla u = h\left(u - u_\infty\right). \tag{28}$$

Here u_∞ will hence be simplified by assuming to be zero. By using the Eq. (21), the Eq. (36b), and the non-equilibrium part of the distribution function in the Eq. (35) up to $O\left(\varepsilon^2\right)$, the following equation reads,

$$f_i = \left(1 + 3h\Delta x\right) f_i^{\text{eq}} \quad \text{for} \quad \left(\mathbf{c}_i\cdot\mathbf{n}\right) > 0. \tag{29}$$

Using the above equation (29) and the following non-equilibrium bounce-back rule:

$$\begin{cases} f_4 - f_4^{\text{eq}} = -\left(f_2 - f_2^{\text{eq}}\right), \\ f_8 - f_8^{\text{eq}} = -\left(f_6 - f_6^{\text{eq}}\right), \\ f_7 - f_7^{\text{eq}} = -\left(f_9 - f_9^{\text{eq}}\right). \end{cases} \tag{30}$$

Finally, the unknown temperature distribution functions are determined in terms of the known temperature distribution functions as follows:

$$\begin{cases} f_4 = \left(\dfrac{2}{1+3h\Delta x} - 1\right)\underline{f_2}, \\ f_8 = \left(\dfrac{2}{1+3h\Delta x} - 1\right)\underline{f_6}, \\ f_7 = \left(\dfrac{2}{1+3h\Delta x} - 1\right)\underline{f_9}, \end{cases} \tag{31}$$

where the underlined terms represent the unknown temperature distribution functions.

3. Validation and numerical example

In this section, several numerical examples are carried out to validate our proposed method. First, in the evaluation of the LBM solver, a direct comparison is performed with a well-established FEM solver. i.e, FreeFEM++ [(45)], though a numerical example to analyze the accuracy of the LBM used in this study. Next, we conduct several numerical examples to evaluate the use of LBM in the topology optimization for the heat conduction problem and its computational efficiency. It is noted that the numerical examples used in this study are motivated by those used in the study by Jing et al. (2015). In the aforementioned study, the authors used BEM for solving the primal and adjoint problems of the optimization while in this study, the primal and adjoint problems are solved by the LBM. It is, however, a direct comparison could not be made because of some different conditions used in the two different simulation methods for the optimization problem.

The termination criterion for evaluating the objective function is given as follows:

$$\frac{\left|J_\varsigma - J_{\varsigma-1}\right|}{J_\varsigma} < \varepsilon_{\text{opt}}, \tag{32}$$

here ς denotes the optimization step, ε_{opt} is set as 10^{-6}. The computation is terminated when the criterion and all the constraints are met.

3.1. Validation

The first numerical example is to solve Laplace's equation. The numerical example is simulated in a square domain (100×100 lattice) used in the LBM approach, which is compatible with the structured mesh (100×100 triangulates unit square) used in the FreeFEM++ tool. The same initial and boundary conditions are applied to both the simulation methods. As described in Fig. 2, the square domain Ω is initially fulfilled with the material, the prescribed boundary condition $\bar{u} = 100$ on the vertical left-most (Γ_u) and the prescribed $\bar{u} = 0$ is applied to the other edges on the right, top, and bottom (Γ_q) of the fixed design domain Ω. While the Galerkin finite element formulation P1 [(45)] is used in the FreeFEM++ tool, some particular conditions are used in the LBM such as the dimensionless relaxation time $\tau_f = 1$, the initial condition of the macroscopic variable $\rho = 0$, and the accuracy is set up to 10^{-6}. For more information on how to implement the FreeFEM++ tool, please refer to the publication by Hecht et al. (2012). We solve the following boundary value problem (BVP) of Laplace's equation:

$$\begin{cases} -\nabla^2 u = 0 & \text{in } \Omega, \\ \bar{u} = 100 & \text{on } \Gamma_u, \\ \bar{u} = 0 & \text{on } \Gamma_q. \end{cases} \tag{33}$$

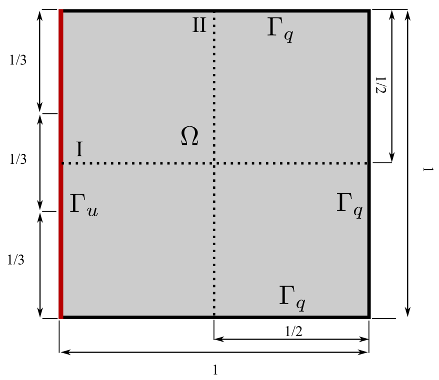

Fig. 2 Design setting of the BVP given by Eq. (33).

With these above settings, we obtained the identical results of Eq. (33) by the two different approaches. As shown in Fig. 3, the similar results of the Laplace problem are achieved by the FreeFEM++ approach and the LBM approach. Furthermore, a direct comparison of the performances between the two methods is conducted to robust the validation of the LBM used in this study. In the comparison, the results of the Laplace problem computed by the FEM solver and the LBM solver are recorded on the centerline I and the centerline II of a square domain (shown in Fig. 2. As shown in Fig. 4, we observed a good agreement in the results obtained by the two different solvers. The finite differences between the results obtained by the two methods are conducted to evaluate the accuracy of the LBM. It is noticed that the relatively small differences of the results achieved by the FEM solver and the LBM solver are computed on both the vertical and horizontal center lines I and II. The finite difference at each lattice point on the center lines I and II are computed by $\left(\frac{|u_L - u_F|}{100}\right)$, where u_L denotes the solution achieved by the LBM and u_F denotes the solution achieved by the FEM at the selected lattice point. To be more specific, a small relative error that is less than 0.0025 on the centerline I is observed while that is less than 0.003 on the centerline II is recorded. This achievement agrees that the LBM can handle the diffusion equation with an acceptable accuracy as a cheap simulation method.

3.2. Numerical example 1

In this numerical example, we aim to minimize a given objective function that is defined on the boundaries of a fixed design domain. The objective function is formulated as follows:

$$J = \int\limits_{\Gamma_h \cup \Gamma_\epsilon} (u - \hat{u})^2 \, d\Gamma, \tag{34}$$

where Γ_ϵ denotes the boundary of the infinitesimal circular removed from the material domain and $\hat{u}$ denotes the target temperature, it is set as $\hat{u} = 10$ in this study.

The fixed design domain is considered as a 50×50 lattice

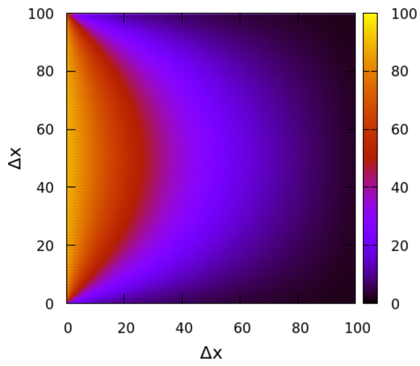

(a) FEM approach

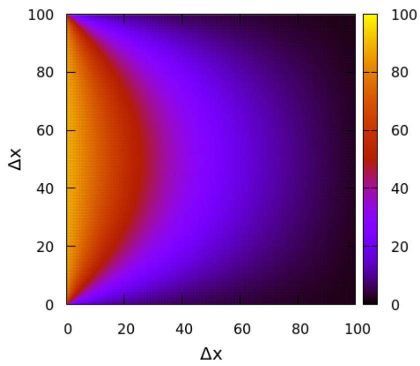

(b) LBM approach

Fig. 3 The results for temperature u calculated by the FEM and LBM.

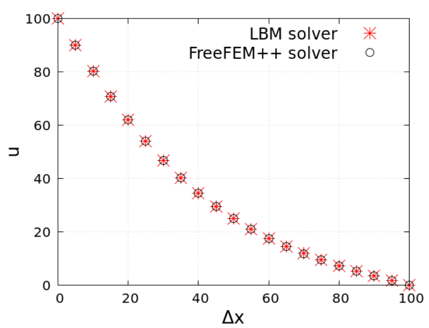

(a) Line I

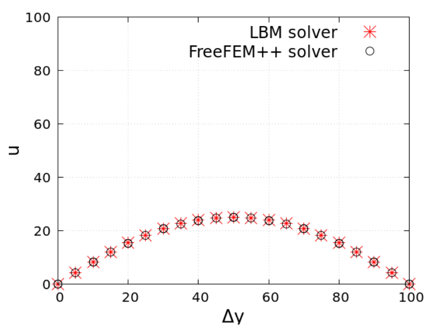

(b) Line II

Fig. 4 The temperatures u calculated at the points along the center lines I and II of the square domain.

square which is initially filled with the material as shown in Fig. 5. The boundary conditions are described in this figure such that the prescribed temperature $\bar{u} = 100$ is imposed on the Dirichlet boundary Γ_D located on each edge of a square domain while the heat transfer coefficient $h = 1$ and the ambient temperature $u_\infty = 0$ are applied to all the Robin boundaries Γ_h. The thermal conductivity is computed by the Eq. (19), the relaxation times $\tau_f = 1$ and $\tau_g = 1$ are used in all numerical examples. The permissible volume constraint of the material V_{max} is set up to 80% of the fixed design domain. The proportional constant $K = 1$ and the regularization $\tau = 5 \times 10^{-3}$ are set for the Eq. (5).

As a result, Fig. 6 shows the optimization histories obtained by the LBM and the BEM at selected optimization time steps. It should be noted that the results obtained by the BEM were produced by Jing et al. (2015) with the same initial and boundary settings excepted the setting parameters (the proportional constant K and the regularization τ) for the time evolution equation Eq. (5) due to the differences of the optimization schemes. For more detail on the settings of the simulation method and the optimization procedure, the readers may refer to the aforementioned publication. The similarities of the optimized configurations obtained by the two methods are observed. To be more specific, a total of 4 holes are appeared and developed to be larger during the optimization. These holes are treated as heat absorbers in which the Robin boundary condition is also applied to their boundary shapes. It is shown in Fig. 8 that the temperature distribution inside these holes is lower than that of the outside in all optimization time steps. They totally complied with the previous study [(17)]. Thus, this confirms that the proposed method can deal with the topology optimization for heat conduction problem and the obtained results can be considered as the solutions.

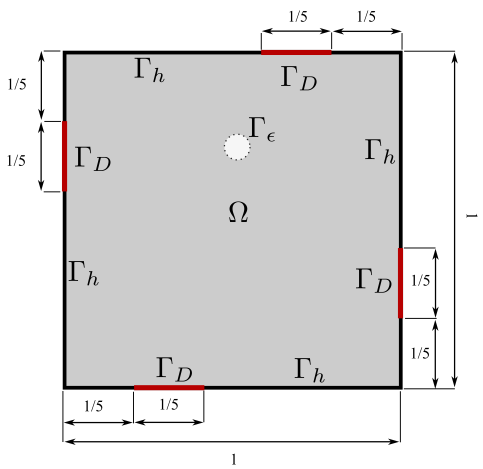

Fig. 5 Design setting of the example 1.

In this numerical example, we also investigated the effect of the regularization parameter to the complexity of the optimal configuration. There are various values of the regularization parameters such as $\tau = 1 \times 10^{-3}$, 5×10^{-3}, and 1×10^{-2} used for the examination. It is shown in Fig. 7, the bigger regularization parameters τ used will create the simpler boundary shapes of the optimal configurations. This is complied with what was found in litteratures [(42)] [(17)].

Figure 9 shows the convergence histories of objective function and the volume constraint. Its smooth convergences confirm the performance of the optimization problem and validate the obtained optimal results. Moreover, to investigate the computational efficiency of the proposed method (using LBM), we ran this numerical example with the same numerical example proposed by Jing et al., 2015 (using BEM) on the same computer. It is noted that the developed codes of the two programs were written in Fortran and run on a PC with Intel Core I7-6700 3.40GHz CPU. As a result, the proposed method took 59 seconds to reach the steady-state while the other took 408 seconds. We observed a significant difference in the computational time by the two studies. The computational time is efficiently saved due to the parallel computation and without using any matrix solver in the LBM program. Therefore, we confirm, as expected, that the effectiveness of using the LBM in topology optimization also for the heat conduction problem.

3.3. Numerical example 2

In the next numerical example, we test the availability of the optimization for a non-square design domain that using the proposed method. In this example, the fixed design domain 100×75 lattice is initially fullfilled by the material with the thermal conductivity calculated by the Eq. (19). The objective function is still defined by the Eq. (34). Literally, the boundary conditions are the same in the prevous numerical example such that the prescribed temperature $\bar{u} = 100$ is imposed on the Dirichlet boundary Γ_D, the heat transfer coefficient $h = 1$, and the ambient temperature $u_\infty = 0$ are used where the Ronbin boundary condition Γ_h applies. The allowable volume V_{max} of the material is 80% of the initial volume. The regularization parameter is chosen as $\tau = 1 \times 10^{-2}$, the relaxation times $\tau_f = 1$ and $\tau_g = 1$ are selected, and the termination criterion is satisfied the Eq. (32).

Figure 12 shows the optimal configuration and its temperature distribution. As what is observed, there are 4 holes were created during the optimization. Their appearences encourage the reduction of the objective function and constraints. Therefore, the proposed method works in the different initial designs, which confirms the potential paradism

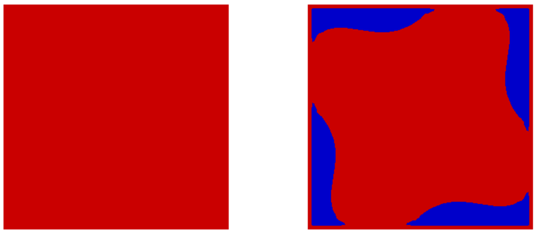

(a) Step = 1 (b) Step = 25

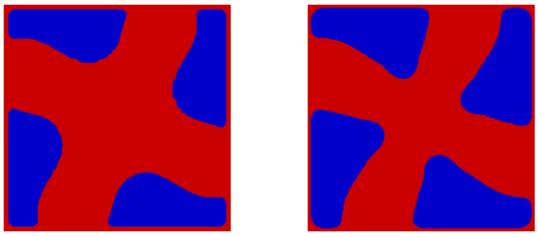

(c) Step = 100 (d) Final step

Case A: Lattice Boltzmann method (produced by this study)

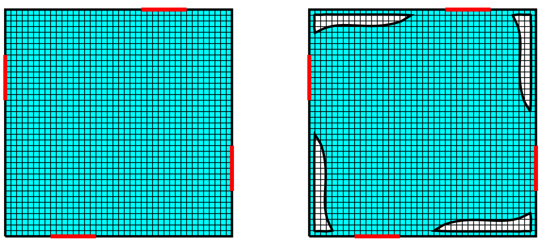

(e) Step = 1 (f) Step = 5

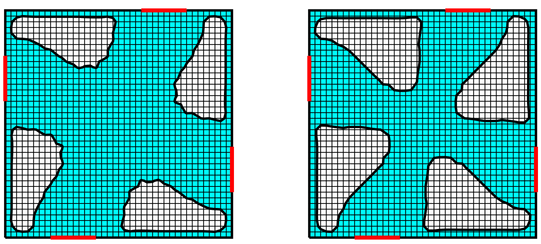

(g) Step = 20 (h) Final step

Case B: Boundary element method (taken from Jing et al., 2015)

Fig. 6 The optimization histories obtained by different approaches.

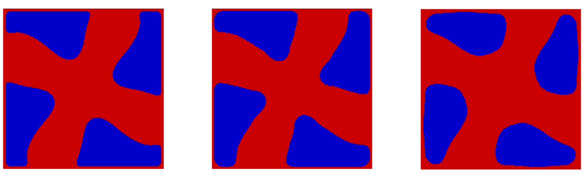

(a) $\tau = 1 \times 10^{-3}$ (b) $\tau = 5 \times 10^{-3}$ (c) $\tau = 1 \times 10^{-2}$

Fig. 7 The different optimized shapes obtained by different regularization parameters τ.

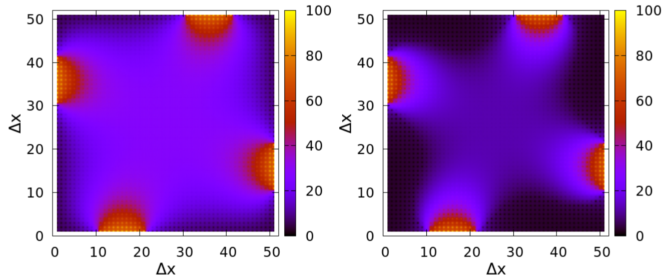

(a) Step = 1 (b) Step = 25

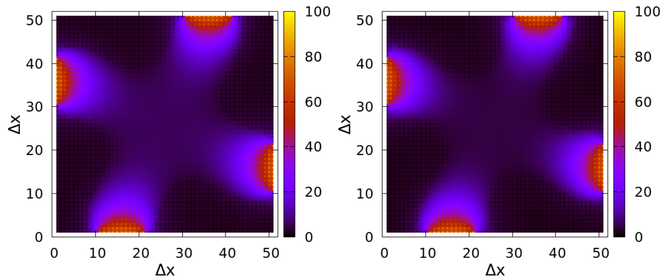

(c) Step = 100 (d) Final step

Fig. 8 The temperature distribution at various steps.

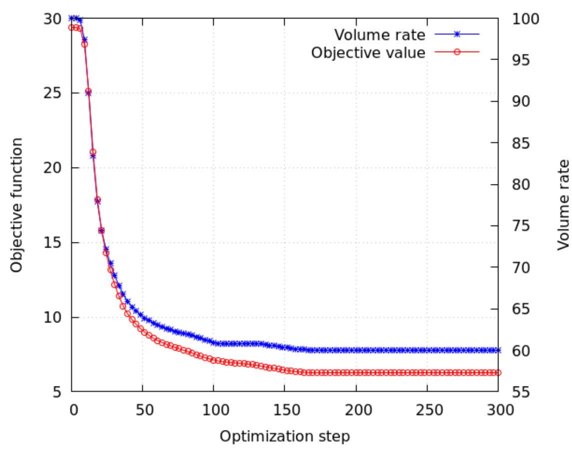

Fig. 9 Convergence histories of objective function and the volume constraint of the example 1.

of the proposed method to deal with various design problems in engineering application. In the future development of the proposed method, the examination for the more complex initial designs will be considered. For those complex shapes, the LBM needs to be developed to deal with the problems of complex geometry.

Figure 11 shows the distribution of normalized topological derivative values. The less regularity of the boundaries between the high-preferable cells (shown in red) and the low-preferable cells (shown in blue) is observed, as compared to the smooth boudaries in the optimal configuration. This however, is explained by the effect of the diffusion term in the time evolution equation (5) for updating the optimal configuration [42]. This penalty behaves via the selection of the regularization parameters in the diffusion term. The more complex shapes will be obtained in an optimization by

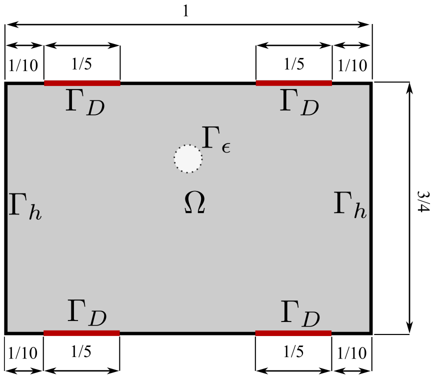

Fig. 10 Design setting of the example 2.

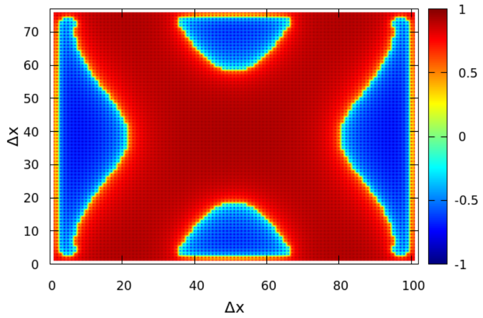

Fig. 11 Distribution of normalized topological derivative values.

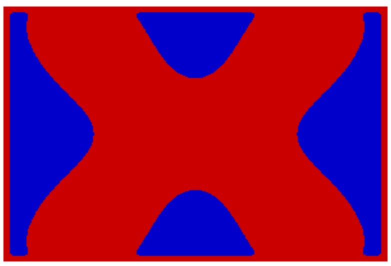

(a) Optimized configuration

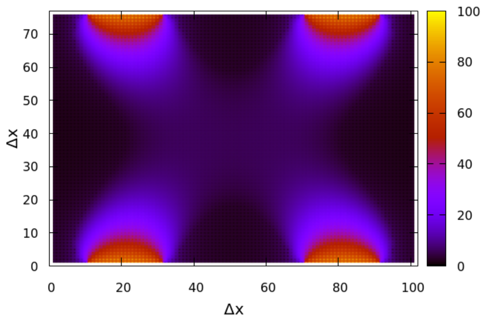

(b) Temperature distribution

Fig. 12 The optimized configuration and its temperature distribution.

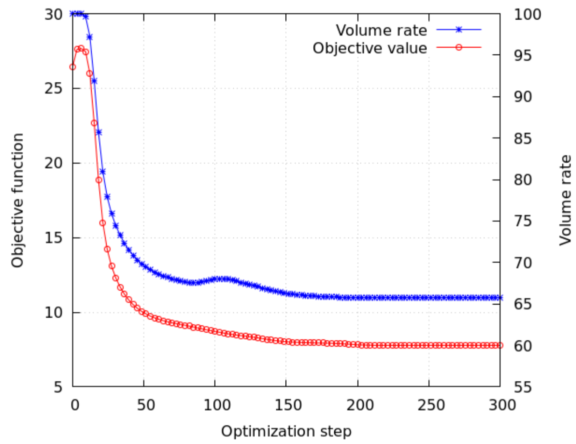

Fig. 13 Convergence histories of objective function and the volume constraint of the example 2.

chosing a relative small value of τ. However, the optimized shapes may be very difficult for manufacturing if it is too complicated. Thus, the reliable results need to be considered by designing an appropriate regularization τ.

Figure 13 shows the convergence histories of objective function and volume constraint in all time steps. The significant reduction of the objective function is noticed when the holes are created inside the fixed design domain, which agrees with the reduction of the volume constraint. The feasible configuration appeared around step 150, however, the total 300 steps are used in this numerical example for a sufficient convergence. The smoothness of the curves certify the obtained results are accepted to be the solutions.

4. Conclusion

In this study, we have successfully proposed a level-set based topology optimization for the heat conduction problem incorporating with the lattice Boltzmann method. The novelty of this study is the primary utilization of the LBM and the topological derivative in a level-set based topology optimization for the heat conduction. The successful cooperation between the LBM and the topological derivative in this study leads this pattern to a potential paradigm for the development of the topology optimization for the fluid flow problem, the thermal-fluid problem, or many other problems in physics. The effectiveness of this method has been performed through numerical examples wherein the optimal solutions obtained by the proposed method properly agreed with the solutions found in the literature. In particular, the performance of the constructed LBM used in this study has been compared with a well-established FEM tool (i.e. the FreeFEM++). The relatively small finite differences between the two methods were observed over a general numerical example. The applicability of the LBM and its computational efficiency in the topology optimization for the heat conduction problem have also been validated by comparing with the results by other conventional methods. The noticeable cutback of the computational time has been observed in the use of LBM for the optimization as compared to a conventional method in the study. The similar optimal results obtained by the two different methods were noticed over various numerical optimization examples. Moreover, due to the limitation in the constructed LBM used in this study, the optimization with more complex boundaries of the initial design could not be performed for testing its stability and accuracy. Specifically, the suitable discretization lattice scheme for the LBM in various initial design problems wherein the Robin boundary condition is employed needs further investigations. It is also noted that the level-set based topology optimization in which the topological derivative is used requires a highly accurate manner for the computation. Thus, the enhancement for accuracy and efficiency of a high-order LBM is essentially demanded. In such a method, the high-order discretization system can be used to improve the current study.

5. Appendix

In this section, the recoveries of the Laplace's equation and Poisson's equation from a chosen LBM pattern are summarized as follows. The Chapman-Enskog analysis is used for the derivation. This gives,

$$\begin{cases} f_i = f_i^{(0)} + \varepsilon f_i^{(1)} + \varepsilon^2 f_i^{(2)} + ..., \\ \dfrac{\partial}{\partial t} = \varepsilon^2 \dfrac{\partial}{\partial t}^{(2)} + ..., \\ \nabla = \varepsilon \nabla^{(1)}, \\ R = \varepsilon^2 R^{(2)}, \end{cases} \tag{35}$$

where $\varepsilon = O\left[\Delta x\right]$. The Taylor analysis is applied to the Eq. (11) in case of recovering Laplace's equation, and applied to the Eq. (12) in case of recovering Poisson's equation.

The results are divided into different orders after expanded by using Chapman-Enskog analysis. As considering up to $O[\Delta x]^2$, it yields,

$$O\left(\varepsilon^o\right): f_i^{(0)} = f_i^{eq}, \tag{36a}$$

$$O\left(\varepsilon^1\right): \left(\mathbf{c}_i \cdot \nabla^{(1)}\right) f_i^{(0)} = -\frac{1}{\tau_f \Delta x} f_i^{(1)}, \tag{36b}$$

$$O\left(\varepsilon^2\right): \left(Sh\frac{\partial}{\partial t}^{(2)}\right) f_i^{(0)} + \left(\mathbf{c}_i \cdot \nabla^{(1)}\right) f_i^{(1)} + \frac{1}{2}\Delta x\left(\mathbf{c}_i \cdot \nabla^{(1)}\right)^2 f_i^{(0)} = -\frac{1}{\tau_f \Delta x} f_i^{(2)}, \tag{36c}$$

where $\Delta t = Sh\Delta x$. Sh denotes the Strouhal number [43].

The Eq. (36c) can be written as follows by using the relation in the Eq. (36b),

$$O\left(\varepsilon^2\right): Sh\frac{\partial}{\partial t}^{(2)} f_i^{(0)} - \Delta x\left(\tau_f - \frac{1}{2}\right)\left(\mathbf{c}_i \cdot \nabla^{(1)}\right)^2 f_i^{(0)} = -\frac{1}{\tau_f \Delta x} f_i^{(2)}. \tag{37}$$

Finally, the Laplace's equation can be recovered by summing up the Eq. (37) and use the relations in Eq. (35),

$$Sh\frac{\partial}{\partial t}u - D_\sigma \nabla^2 u = 0, \tag{38}$$

where $\sum_{i=1}^{9} f_i^{(k)} = 0 \ (k \geq 1)$ is implicitly used.

Similarly, the Poisson's equation can be recovered by using the same above procedures. The result of the time evolution equation in second order is written as follows:

$$O\left(\varepsilon^2\right): Sh\frac{\partial}{\partial t}^{(2)} g_i^{(0)} - \Delta x\left(\tau_g - \frac{1}{2}\right)\left(\mathbf{c}_i \cdot \nabla^{(1)}\right)^2 g_i^{(0)} = -\frac{1}{\tau_g \Delta x} g_i^{(2)} + w_i R^{(2)} D_{\sigma^*}. \tag{39}$$

Since $\sum_{i=1}^{9} g_i^{(k)} = 0 \ (k \geq 1)$, the Poisson's equation is recovered by summing the Eq. (39) as follows:

$$Sh\frac{\partial}{\partial t}\mu - D_{\sigma^*} \nabla^2 \mu = RD_{\sigma^*}. \tag{40}$$

It is noted that in the steady problem, the time derivatives in the Eq. (38) and the Eq. (40) should be ignored.

References

(1) Alberto Donoso and Pablo Pedregal. Optimal design of 2D conducting graded materials by minimizing quadratic functionals in the field. *Structural and Multidisciplinary Optimization*, Vol. 30, No. 5, pp. 360–367, 2005.

(2) Allan Gersborg-Hansen, Martin P Bendsøe, and Ole Sigmund. Topology optimization of heat conduction problems using the finite volume method. *Structural and Multidisciplinary Optimization*, Vol. 31, No. 4, pp. 251–259, 2006.

(3) Ercan Mehmet Dede. Multiphysics topology optimization of heat transfer and fluid flow systems. In *Proceedings of The COMSOL Users Conference*, 2009.

(4) Gilles Marck, Maroun Nemer, Jean-Luc Harion, Serge Russeil, and Daniel Bougeard. Topology optimization using the SIMP method for multiobjective conductive problems. *Numerical Heat Transfer, Part B: Fundamentals*, Vol. 61, No. 6, pp. 439–470, 2012.

(5) Jaco Dirker and Josua Petrus Meyer. Topology optimization for an internal heat-conduction cooling scheme in a square domain for high heat flux applications. *Journal of Heat Transfer*, Vol. 135, No. 11, pp. 111010–10, 2013.

(6) Francois H Burger, Jaco Dirker, and Josua Petrus Meyer. Three-dimensional conductive heat transfer topology optimisation in a cubic domain for the volume-to-surface problem. *International Journal of Heat and Mass Transfer*, Vol. 67, pp. 214–224, 2013.

(7) Suna Yan, Fengwen Wang, and Ole Sigmund. On the non-optimality of tree structures for heat conduction. *International Journal of Heat and Mass Transfer*, Vol. 122, pp. 660–680, 2018.

(8) Shuhao Wu, Yongcun Zhang, and Shutian Liu. Topology optimization for minimizing the maximum temperature of transient heat conduction structure. *Structural and Multidisciplinary Optimization*, Vol. 60, No. 1, pp. 69–82, 2019.

(9) Lei Tang, Tong Gao, Longlong Song, Liang Meng, Chengqi Zhang, and Weihong Zhang. Topology optimization of nonlinear heat conduction problems involving large temperature gradient. *Computer Methods in Applied Mechanics and Engineering*, Vol. 357, p. 112600, 2019.

(10) Gil Ho Yoon, Ercan Mehmet Dede, Tsuyoshi Nomura, and Paul Schmalenberg. Topology optimization of time-transient heat conduction for thermo-optic silicon modulators. *International Journal of Heat and Mass Transfer*, Vol. 157, p. 119862, 2020.

(11) Qing Li, Grant P Steven, Yi Min Xie, and Osvaldo M Querin. Evolutionary topology optimization for temperature reduction of heat conducting fields. *International Journal of Heat and Mass Transfer*, Vol. 47, No. 23, pp. 5071–5083, 2004.

(12) Tong Gao, Weihong Zhang, Jihong Zhu, Yingjie Xu, and David H Bassir. Topology optimization of heat conduction problem involving design-dependent heat load effect. *Finite Elements in Analysis and Design*, Vol. 44, No. 14, pp. 805–813, 2008.

(13) Seung-Hyun Ha and Seonho Cho. Topological shape optimization of heat conduction problems using level set approach. *Numerical Heat Transfer, Part B: Fundamentals*, Vol. 48, No. 1, pp. 67–88, 2005.

(14) ChunGang Zhuang, ZhenHua Xiong, and Han Ding. A level set method for topology optimization of heat conduction problem under multiple load cases. *Computer Methods in Applied Mechanics and Engineering*, Vol. 196, No. 4-6, pp. 1074–1084, 2007.

(15) Takayuki Yamada, Kazuhiro Izui, and Shinji Nishiwaki. A level set-based topology optimization method for maximizing thermal diffusivity in problems including design-dependent effects. *Journal of Mechanical Design*, Vol. 133, No. 3, pp. 031011–9, 2011.

(16) Guoxian Jing, Toshiro Matsumoto, Toru Takahashi, Hiroshi Isakari, and Takayuki Yamada. Topology optimization for 2D heat conduction problems using boundary element method and level set method. *Transactions of JASCOME*, Vol. 13, No. 19, pp. 5–10, 2013.

(17) Guoxian Jing, Hiroshi Isakari, Toshiro Matsumoto, Takayuki Yamada, and Toru Takahashi. Level set-based topology optimization for 2D heat conduction problems using BEM with objective function defined on design-dependent boundary with heat transfer boundary condition. *Engineering Analysis with Boundary Elements*, Vol. 61, pp. 61–70, 2015.

(18) Benliang Zhu, Xianmin Zhang, Nianfeng Wang, and Sergej Fatikow. Optimize heat conduction problem using level set method with a weighting based velocity constructing scheme. *International Journal of Heat and Mass Transfer*, Vol. 99, pp. 441–451, 2016.

(19) Talib Dbouk. A review about the engineering design of optimal heat transfer systems using topology optimization. *Applied Thermal Engineering*, Vol. 112, pp. 841–854, 2017.

(20) Shiyi Chen and Gary D Doolen. Lattice Boltzmann method for fluid flows. *Annual Review of Fluid Mechanics*, Vol. 30, No. 1, pp. 329–364, 1998.

(21) Zhaoli Guo, Baochang Shi, and Nengchao Wang. Lattice BGK model for incompressible Navier-Stokes equation. *Journal of Computational Physics*, Vol. 165, No. 1, pp. 288–306, 2000.

(22) Masato Yoshino, Yasuhiro Matsuda, and Changcheng Shao. Comparison of accuracy and efficiency between the lattice Boltzmann method and the finite difference method in viscous/thermal fluid flows. *International Journal of Computational Fluid Dynamics*, Vol. 18, No. 4, pp. 333–345, 2004.

(23) XF Pan, Aiguo Xu, Guangcai Zhang, and Song Jiang. Lattice Boltzmann approach to high-speed compressible flows. *International Journal of Modern Physics C*, Vol. 18, No. 11, pp. 1747–1764, 2007.

(24) FL Hinton, MN Rosenbluth, SK Wong, YR Lin-Liu, and RL Miller. Modified lattice Boltzmann method for compressible fluid simulations. *Physical Review E*, Vol. 63, No. 6, p. 061212, 2001.

(25) Moran Wang and Qinjun Kang. Modeling electrokinetic flows in microchannels using coupled lattice Boltzmann methods. *Journal of Computational Physics*, Vol. 229, No. 3, pp. 728–744, 2010.

(26) Jianying Zhang, Guangwu Yan, and Yinfeng Dong. A new lattice Boltzmann model for the Laplace equation. *Applied Mathematics and Computation*, Vol. 215, No. 2, pp. 539–547, 2009.

(27) Aksel Hiorth, UH a Lad, S Evje, and SM Skjaeveland. A lattice Boltzmann-BGK algorithm for a diffusion equation with robin boundary condition-application to NMR relaxation. *International journal for Numerical Methods in Fluids*, Vol. 59, No. 4, pp. 405–421, 2009.

(28) Miki Hirabayashi, Yu Chen, and Hirotada Ohashi. The lattice BGK model for the Poisson equation. *JSME International Journal Series B Fluids and Thermal Engineering*, Vol. 44, No. 1, pp. 45–52, 2001.

(29) Zhenhua Chai and Baochang Shi. A novel lattice Boltzmann model for the Poisson equation. *Applied Mathematical Modelling*, Vol. 32, No. 10, pp. 2050–2058, 2008.

(30) Jinku Wang, Moran Wang, and Zhixin Li. Lattice Poisson-Boltzmann simulations of electro-osmotic flows in microchannels. *Journal of Colloid and Interface Science*, Vol. 296, No. 2, pp. 729–736, 2006.

(31) Jianying Zhang and Guangwu Yan. A lattice Boltzmann model for the reaction-diffusion equations with higher-order accuracy. *Journal of Scientific Computing*, Vol. 52, No. 1, pp. 1–16, 2012.

(32) Georg Pingen, Anton Evgrafov, and Kurt Maute. Topology optimization of flow domains using the lattice Boltzmann method. *Structural and Multidisciplinary Optimization*, Vol. 34, No. 6, pp. 507–524, 2007.

(33) Geng Liu, Martin Geier, Zhenyu Liu, Manfred Krafczyk, and Tao Chen. Discrete adjoint sensitivity analysis for fluid flow topology optimization based on the generalized lattice Boltzmann method. *Computers & Mathematics with Applications*, Vol. 68, No. 10, pp. 1374–1392, 2014.

(34) Kentaro Yaji, Takayuki Yamada, Masato Yoshino, Toshiro Matsumoto, Kazuhiro Izui, and Shinji Nishiwaki. Topology optimization using the lattice Boltzmann method incorporating level set boundary expressions. *Journal of Computational Physics*, Vol. 274, pp. 158–181, 2014.

(35) Andrew Kirk, Sebastian Kreissl, Georg Pingen, and Kurt Maute. Lattice Boltzmann topology optimization for transient flow. In *MAESC 2011 Conference May*, Vol. 3, 2011.

(36) Sebastian Nørgaard, Ole Sigmund, and Boyan Lazarov. Topology optimization of unsteady flow problems using the lattice Boltzmann method. *Journal of Computational Physics*, Vol. 307, pp. 291–307, 2016.

(37) Cong Chen, Kentaro Yaji, Takayuki Yamada, Kazuhiro Izui, and Shinji Nishiwaki. Local-in-time adjoint-based topology optimization of unsteady fluid flows using the lattice Boltzmann method. *Mechanical Engineering Journal*, Vol. 4, No. 3, pp. 17–00120, 2017.

(38) Truong Nguyen, Hiroshi Isakari, Toru Takahashi, Kentaro Yaji, Masato Yoshino, and Toshiro Matsumoto. Level-set based topology optimization of transient flow using lattice Boltzmann method considering an oscillating flow condition. *Computers & Mathematics with Applications*, Vol. 80, No. 1, pp. 82–108, 2020.

(39) Jacek Rokicki, et al. Adjoint lattice Boltzmann for topology optimization on multi-GPU architecture. *Computers & Mathematics with Applications*, Vol. 71, No. 3, pp. 833–848, 2016.

(40) Kentaro Yaji, Takayuki Yamada, Masato Yoshino, Toshiro Matsumoto, Kazuhiro Izui, and Shinji Nishiwaki. Topology optimization in thermal-fluid flow using the lattice Boltzmann method. *Journal of Computational Physics*, Vol. 307, pp. 355–377, 2016.

(41) Florian Dugast, Yann Favennec, Christophe Josset, Yilin Fan, and Lingai Luo. Topology optimization of thermal fluid flows with an adjoint lattice Boltzmann method. *Journal of Computational Physics*, Vol. 365, pp. 376–404, 2018.

(42) Takayuki Yamada, Kazuhiro Izui, Shinji Nishiwaki, and Akihiro Takezawa. A topology optimization method based on the level set method incorporating a fictitious interface energy. *Computer Methods in Applied Mechanics and Engineering*, Vol. 199, No. 45-48, pp. 2876–2891, 2010.

(43) Masato Yoshino and Takaji Inamuro. Lattice Boltzmann simulations for flow and heat/mass transfer problems in a three-dimensional porous structure. *International Journal for Numerical Methods in Fluids*, Vol. 43, No. 2, pp. 183–198, 2003.

(44) Takaji Inamuro. A lattice kinetic scheme for incompressible viscous flows with heat transfer. *Philosophical Transactions of the Royal Society of London. Series A: Mathematical, Physical and Engineering Sciences*, Vol. 360, No. 1792, pp. 477–484, 2002.

(45) Frédéric Hecht. New development in freefem++. *Journal of Numerical Mathematics*, Vol. 20, No. 3-4, pp. 1–14, 2012.